PHYSICAL REVIEW B **85**, 100409(R) (2012)

Phase locking dynamics of dipolarly coupled vortex-based spin transfer oscillators

A. D. Belanovsky,[1] N. Locatelli,[2] P. N. Skirdkov,[1] F. Abreu Araujo,[3] J. Grollier,[2] K. A. Zvezdin,[1,4] V. Cros,[2] and A. K. Zvezdin[1]

[1]*A. M. Prokhorov General Physics Institute, RAS, Vavilova, 38, 119991 Moscow, Russia*

[2]*Unité Mixte de Physique CNRS/Thales, 1 avenue A. Fresnel, 91767 Palaiseau, France and Université Paris–Sud, 91405 Orsay, France*

[3]*Université Catholique de Louvain, 1 place de l'Université, 1348 Louvain-la-Neuve, Belgium*

[4]*Istituto P.M. srl, via Grassi, 4, 10138 Torino, Italy*

(Received 5 November 2011; revised manuscript received 11 March 2012; published 30 March 2012)

Phase locking dynamics of dipolarly coupled vortices excited by spin-polarized current in two identical nanopillars is studied as a function of the interpillar distance L. Numerical study and an analytical model have proved the remarkable efficiency of magnetostatic interaction in achieving phase locking. Investigating the dynamics in the transient regime toward phase locking, we extract the evolution of the locking time τ, the coupling strength μ, and the interaction energy W. Finally, we compare this coupling energy with the one obtained by a simple model.

DOI: 10.1103/PhysRevB.85.100409 PACS number(s): 85.75.−d

Injecting a spin-polarized current through magnetic multilayers leads to a new interesting physical phenomenon called the spin transfer effect. These interactions between the spins of charge carriers and local magnetic moments create an additional torque exerted on the magnetization.[1] As a result, a complex spin-transfer-driven magnetic dynamics is revealed with characteristic bifurcations of the Poincaré-Andronov-Hopf type, and limit cycles arise in this highly nonequilibrium medium. The diversity of these new effects is especially true for systems of interacting nanomagnets, penetrated by spin-polarized current. One of the novel effects is the current-driven magnetization oscillations,[2] which might lead to tantalizing possibilities for new nanoscale microwave devices with frequencies that are tunable over a wide range using applied currents and fields. While many crucial advances have been made in the fabrication and understanding of such spin transfer nano-oscillators (STNOs), there remain several critical problems yet to be resolved, in particular the low microwave power and quality factor of a single STNO.

To tackle these issues, particular attention has been focused recently on vortex STNOs that could present a significant output power,[3] a very small spectral linewidth,[4] and/or large frequency agilities at zero field.[5] Moreover, several encouraging experiments have been reported on the vortices phase-locking through exchange interaction[6] and synchronization to external microwave current.[7] Beyond these practical interests, a magnetic vortex and its dynamical modes,[8] notably the gyrotropic motion of the vortex core, is a model system for investigation thoroughly the physics of the spin transfer torque acting on a highly nonuniform magnetic configuration.[9,10] Collective gyrotropic modes are a mean to improve drastically the spectral coherence of any oscillator system.[11] Similarly, vortex-based systems can be chosen to be a new playground for investigation of the influence of the magnetostatic interactions on the collective behavior of vortices.

The collective dynamics of magnetostatically coupled vortices has been studied both experimentally and theoretically for the case of low-amplitude oscillations excited by means of external rf magnetic field[12–16] and spin-polarized current.[17,18] However, none of these models are applicable to the case of interest, i.e., the large-amplitude steady oscillations. The fundamental reason is the hypothesis of low-amplitude oscillations near the centers of nanodots used by these models. A strong consequence of this approximation is that mathematically it allows us to use the ratio of the vortex orbit to the disk radii as a small parameter. However, in the case of the phase locking of the large-amplitude oscillations, such linearization is due neither to the vortex STNOs nor to the uniform ones.[19] In this paper, we propose a model for the dynamics of the coupled vortices without using this assumption. This model provides an expression for the coupling energy with the parameters of the transient process, which can be directly determined either through micromagnetic simulations or by experiment.

The studied system consists of two identical nanopillars with diameters 200 nm, each of them being composed by a free magnetic layer, a nonmagnetic spacer, and a synthetic antiferromagnet (SAF) polarizer that generates a perpendicular spin polarization p_z (see Fig. 1). In our simulations, we consider these layers only by the value of spin polarization, as in Ref. 17, since SAF polarizers that are widely used in vortex STNO experiments have a negligible magnetostatic field, and thus have almost no influence on the dynamics of the vortices.

A free layer is $h = 10$ nm thick $Ni_{81}Fe_{19}$ and has a magnetic vortex as a ground state. The magnetic parameters of the free layer are the magnetization $M_s = 800$ emu/cm^3, the exchange energy $A = 1.3 \times 10^{-6}$ erg/cm, and the damping parameter $\alpha = 0.01$. In order to be above the critical current, a spin polarization P of 0.2 and a current density J of 7×10^6 A/cm^2 have been chosen. The initial magnetic configuration is two centered vortices with the same core polarities and chiralities. The micromagnetic simulations are performed by numerical integration of the Landau-Lifshitz-Gilbert (LLG) equation using our micromagnetic code SPINPM based on the fourth-order Runge-Kutta method with an adaptive time-step control for the time integration and a mesh size 2.5×2.5 nm^2.

In this work, the evolution of the phase locking dynamics as a function of the interpillar distance has been studied. To that end, a series of micromagnetic simulations with different distances L (50, 100, 200, and 500 nm) have been performed. The results of the simulations are then analyzed to extract the radius of the vortex core trajectory in each free layer as well as the phase difference ψ between core radius vectors as a function of time.

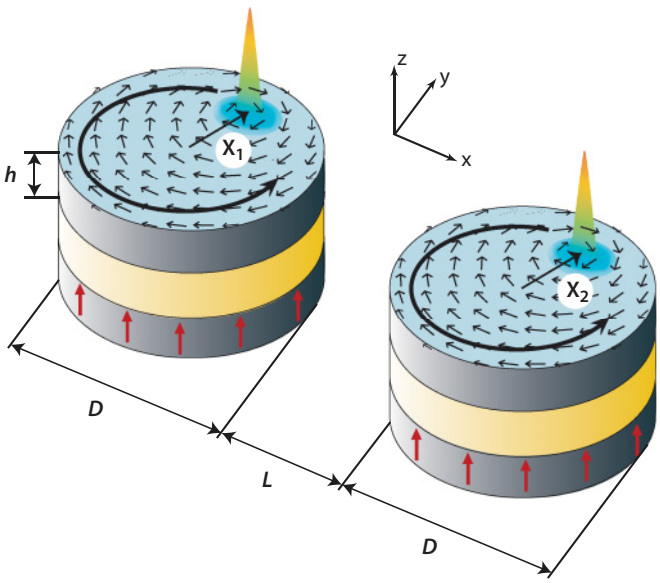

FIG. 1. (Color online) Schematic representation of two interacting spin transfer oscillators. Each pillar is composed of a free magnetic layer with a vortex, a nonmagnetic spacer, and a SAF polarizer. Red arrows indicates the direction of spin polarization created by the polarizer. The nanopillars have a diameter $D = 2R_D =$ 200 nm and are separated by a distance L. The parameters $\mathbf{X}_1$ and $\mathbf{X}_2$ define the core positions.

In Fig. 2, the simulation results for $L = 50$ nm are presented. The transient dynamics of the vortices can be divided into two regimes. At $t = 0$, the spin torque is switched on and thus the radii of both core trajectories increase toward their equilibrium orbits for about 300 ns [see Fig. 2(a)]. The phase difference between the two radius vectors shown in Fig. 2(b) remains constant and equal to $-\pi$ because of the repulsive core-core interaction. The second regime begins when the two cores have reached orbits close to their steady

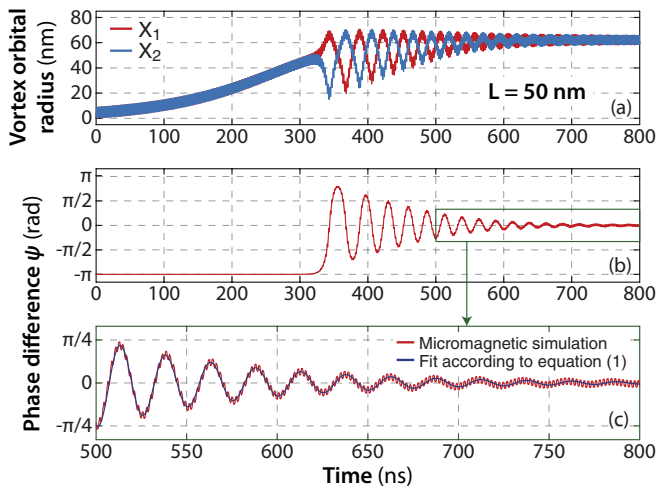

FIG. 2. (Color online) Micromagnetic simulations for $L = 50$ nm of the phase locking dynamics. Evolution as a function of time t of the vortex core orbital positions X_1 and X_2 (a) and the phase difference ψ (b). In (c), a zoom of the phase difference ψ is presented for the time window in which the fitting with Eq. (1) has been done.

TABLE I. Values of the phase difference frequency Ω, the phase locking time τ, and the steady-state radius of the core motion X_0 at different interpillar distances L using the expression of Eq. (1).

L (nm)	Ω (MHz)	τ (ns)	X_0 (nm)
50	40.134	82.59	63.59
100	28.305	85.28	62.46
200	17.183	89.57	61.82
500	7.018	90.13	61.53

ones. From this stage, both the intercore distance and the phase difference [see Figs. 2(a) and 2(b)] exhibit large oscillations, indicating the beginning of the phase locking.

The second regime is one of fundamental interest for this work since the coupling energy can be extracted using the analysis of the core motion in this transient regime [indicated by the square in Fig. 2(b)]. During this time range, the phase difference ψ can be identified as being a low-frequency damped oscillation described by the following expression:

$$\psi = e^{-\frac{t}{\tau}+C_1}\sin(\Omega t + C_2). \tag{1}$$

As shown in Fig. 2(c) and Fig. 3, the fitting is done for the time window between 500 and 800 ns in which the mean orbit radii have reached the common equilibrium value X_0. From the fitting, one can extract for $L = 50$ nm a frequency Ω equal to 40.134 MHz and a phase locking time of 82.59 ns.

The parameters extracted from the fitting procedure for all the interdot distances are summarized in Table I. One should note that the phase locked equilibrium orbit radius X_0 does not vary much with L (see Fig. 3).

To derive the coupling energy between the oscillators from the simulations, we have developed an analytical model based on Thiele equations[20] coupled through the dipolar interaction energy W_{int}.[21–23] Due to the system symmetry, the interaction energy can be expressed as $W_{\text{int}} = a_1x_1x_2 + b_1y_1y_2$, which can be reformulated using the core positions $\boldsymbol{X}_1$ and $\boldsymbol{X}_2$ as[24]

$$W_{\text{int}}(\mathbf{X}_1,\mathbf{X}_2) = \mu_1\mathbf{X}_1\cdot\mathbf{X}_2 + \mu_2(x_1x_2 - y_1y_2), \tag{2}$$

where $\mu_{1,2}$ are the interaction parameters and $x_{1,2}, y_{1,2}$ are core coordinates. The second term of Eq. (2) is neglected in our study since it corresponds only to fast oscillations at double frequency of the gyrotropic modes and thus is averaged over the low-frequency dynamics, which is responsible for

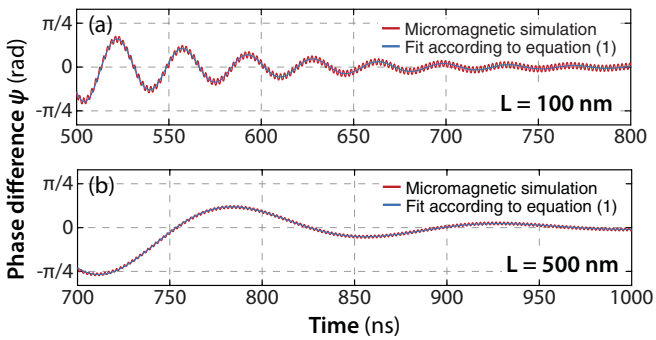

FIG. 3. (Color online) Phase difference ψ as a function of time t for different interpillar distances $L = 100$ (a) and $L = 500$ nm (b).

the phase locking. As a consequence, the expression for the interaction energy can be written as $W_{\rm int}(\mathbf{X}_1,\mathbf{X}_2) = \mu \mathbf{X}_1 \cdot \mathbf{X}_2$.

The two Thiele equations of the core dynamics considering both the spin-transfer torque and the interaction between the two oscillators are

$$G(\mathbf{e}_z \times \dot{\mathbf{X}}_{1,2}) - k_{1,2}(\mathbf{X})\mathbf{X} - \hat{D}\dot{\mathbf{X}}_{1,2} - \mathbf{F}_{\rm STT} - \mathbf{F}_{\rm int} = \mathbf{0}. \quad (3)$$

The first three terms are the conventional forces: the gyrotropic force with $G\mathbf{e}_z = -2\pi p \frac{M_s h}{\gamma}\mathbf{e}_z$, the confining force with $k(\mathbf{X}) = \omega_0 G(1 + a\frac{\mathbf{X}^2}{R_D^2})$,[25,26] where the gyrotropic frequency is $\omega_0 = \frac{20}{9}\gamma M_s h/R$, and the dyadic damping $\hat{D} = \alpha\eta G, \eta = \frac{1}{2}\ln(\frac{R_D}{2l_0}) + \frac{3}{8}$, where $l_0 = \sqrt{\frac{A}{2\pi M_s^2}}$. The fourth term $\mathbf{F}_{\rm STT}$ is the spin transfer force. For the case of a uniform perpendicularly magnetized polarizer, $\mathbf{F}_{\rm STT} = \pi\gamma a_J M_s h(\mathbf{e}_z \times \mathbf{X}) = \varkappa(\mathbf{e}_z \times \mathbf{X})$,[9] where the spin torque amplitude is $a_J = PJ/M_s h$ with P the spin polarization and J the current density. The last term describes the interaction forces and is expressed by $\mathbf{F}_{\rm int}(\mathbf{X}_{1,2}) = -\partial W_{\rm int}(\mathbf{X}_1,\mathbf{X}_2)/\partial \mathbf{X}_{1,2} = -\mu \mathbf{X}_{2,1}$. These Thiele equations can be reformulated in polar coordinates as (using $\alpha\eta \ll 1$)

$$\frac{\dot{X}_1}{X_1} = -\left(\frac{\alpha\eta k_1(X_1) + \varkappa}{G}\right) + \frac{\mu}{G}\frac{X_2}{X_1}(\sin\psi - \alpha\eta\cos\psi), \quad (4)$$

$$\frac{\dot{X}_2}{X_2} = -\left(\frac{\alpha\eta k_2(X_2) + \varkappa}{G}\right) - \frac{\mu}{G}\frac{X_1}{X_2}(\sin\psi + \alpha\eta\cos\psi), \quad (5)$$

$$\dot{\psi} = a\omega_0\left(\frac{X_2^2 - X_1^2}{R_D^2}\right) - \alpha\eta\left(\frac{\dot{X}_1}{X_1} - \frac{\dot{X}_2}{X_2}\right) - \frac{\mu}{G}\cos\psi\left(\frac{X_2}{X_1} - \frac{X_1}{X_2}\right). \quad (6)$$

These two equations of the core motion and the equation of the phase difference provide a complete dynamical description of the phase locking. By linearizing Eqs. (4)–(6) with the assumptions that $\psi \ll 1$ and $\varepsilon = \frac{X_1 - X_2}{X_1 + X_2} \ll 1$, we obtain

$$\dot{\varepsilon} = 2\alpha\eta\left(\tilde{\mu} - \omega_0 a r_0^2\right)\varepsilon + \tilde{\mu}\psi, \quad (7)$$

$$\dot{\psi} = 4\left(\tilde{\mu} - \omega_0 a r_0^2\right)\varepsilon - 2\alpha\eta\tilde{\mu}\psi, \quad (8)$$

where we used $\tilde{\mu} = \mu/G$ and $r_0 = X_0/R_D$. Equations (7) and (8) are linear and their eigenvalues are

$$\lambda_{1,2} = \alpha\eta\omega_0 a r_0^2 \pm \sqrt{\alpha^2\eta^2\omega_0^2\left(a r_0^2\right)^2 + 4\tilde{\mu}^2 - 4\tilde{\mu}\omega_0 a r_0^2}. \quad (9)$$

First we consider the case of periodic solutions when $\frac{1}{2}(\omega_0 a r_0^2 - \omega_0 a r_0^2\sqrt{1-\alpha^2\eta^2}) < \tilde{\mu} < \frac{1}{2}(\omega_0 a r_0^2 + \omega_0 a r_0^2\sqrt{1-\alpha^2\eta^2})$. The eigenvalues can thus be written as

$$1/\tau = \alpha\eta\omega_0 a r_0^2, \quad (10)$$

$$\Omega^2 = -\alpha^2\eta^2\omega_0^2\left(a r_0^2\right)^2 - 4\tilde{\mu}^2 + 4\tilde{\mu}\omega_0 a r_0^2. \quad (11)$$

The important result of this study is that Eqs. (10) and (11) allow us to connect the coupling parameter μ with the phase locking parameters, i.e., Ω and τ, obtained through micromagnetic simulations. Consequently, an expression of the time-averaged interaction energy $W_{\rm int}$ takes the form $W_{\rm int}(L) = \mu X_0^2 = \frac{G}{2}[1/(\tau\alpha\eta) - \sqrt{1/(\tau\alpha\eta)^2 - \Omega(L)^2}]X_0^2$. In Fig. 4, the evolution of this interaction energy $W_{\rm int}$ with the interpillar separation distance D_{12} derived from micromagnetic modeling is displayed by blue square dots. We obtain the best fit for an energy decay law as $D_{12}^{-3.6}$. In comparison, in the case of small core amplitudes[12,13] this decay law has been found as D_{12}^{-6}, however this was not confirmed experimentally.[17]

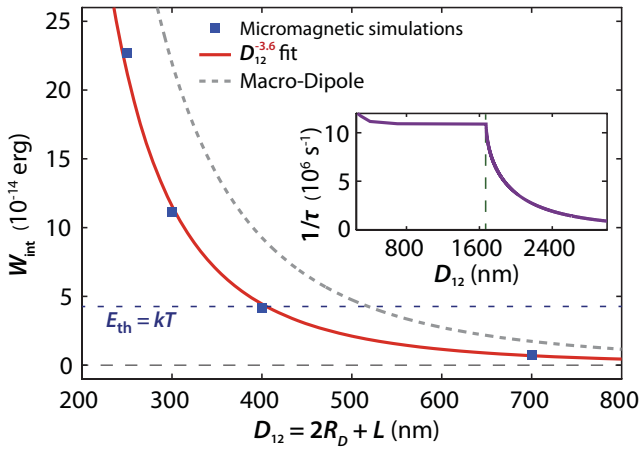

FIG. 4. (Color online) Absolute values of interaction energy $W_{\rm int}$ as a function of interpillar separation distance $D_{12} = 2R_D + L$ obtained from the micromagnetic simulations (blue square dots) and from the macrodipole model (red solid line). Inset: Evolution of the phase locking rate $1/\tau$ vs D_{12} (purple solid line).

To get more insight into the origin of this large coupling interaction, the values of the interaction energy $W_{\rm int}$ obtained by simulations are compared with those derived from a simple model of two interacting macrodipoles, concentrated at the dot centers and rotating at a frequency ω_0. In such a case, the magnetic dipole interaction energy $W_{\rm int}^{\rm md}$ is defined as

$$W_{\rm int}^{\rm md} = \frac{(\mathbf{M}_1 \cdot \mathbf{M}_2)}{D_{12}^3}V_D^2 - \frac{3(\mathbf{M}_1 \cdot \mathbf{D}_{12})(\mathbf{M}_2 \cdot \mathbf{D}_{12})}{D_{12}^5}V_D^2, \quad (12)$$

where $D_{12} = 2R_D + L$. The in-plane magnetization $\mathbf{M}_{1,2}$ is perpendicular to the radius vector of the core position, thus one can write $\mathbf{M}_{1,2} = \zeta(\mathbf{X}_{1,2} \times \mathbf{e}_z)$, where ζ is a constant that has been numerically calculated: $\zeta \approx 5.6$ G/nm. The interaction energy can be rewritten in the following form:

$$W_{\rm int}^{\rm md} = \underbrace{A\mathbf{X}_1\mathbf{X}_2}_{\text{low-frequency oscillations}} + \underbrace{BX_1X_2\cos(\varphi_1 + \varphi_2)}_{\text{high-frequency dynamics}} \quad (13)$$

with $A = -\frac{\zeta^2 V_D^2}{2D_{12}^3}, B = \frac{3}{2}\frac{\zeta^2 V_D^2}{D_{12}^3}$. As far as the phase locking dynamics is concerned, the second term in Eq. (13) corresponding to high-frequency oscillations is averaged to zero and thus one can express the mean interaction energy $W_{\rm int}^{\rm md}$ in the macrodipole approximation:

$$W_{\rm int}^{\rm md} = -\frac{\zeta^2 V_D^2}{2D_{12}^3}\mathbf{X}_1\mathbf{X}_2 = \mu^{\rm md}\mathbf{X}_1\mathbf{X}_2. \quad (14)$$

In Fig. 4, we observe that for small interpillar distances, $W_{\rm int}$ differs significantly from the macrodipole energy $W_{\rm int}^{\rm md}$. This difference demonstrates the importance of the magnetic quadrupole and higher multipoles for the phase locking dynamics.

Coming back to Eqs. (7) and (8), a second regime has to be considered when $\tilde{\mu} < \frac{1}{2}(\omega_0 a r_0^2 - \omega_0 a r_0^2\sqrt{1-\alpha^2\eta^2})$ or

$\tilde{\mu} > \frac{1}{2}(\omega_0 a r_0^2 + \omega_0 a r_0^2 \sqrt{1-\alpha^2\eta^2})$. In this case, the solutions are aperiodic oscillations and they strongly impact the main features of the phase locking, notably the phase locking rate $1/\tau$. Indeed, in the regime of periodic oscillations, this phase locking parameter is almost independent of the coupling strength μ (see Fig. 3) for interpillar separation distance D_{12} values as large as 1600 nm (see the inset of Fig. 4). We emphasize that the weak variation of the phase locking rate obtained in the micromagnetic simulations (see the values in Table I) is in fact solely due to the small variations of the steady orbit radii X_0 with the interpillar distance L as expected from (10). On the contrary, in the aperiodic regime, the phase locking rate $1/\tau$ depends strongly on the coupling strength μ with the following expression:

$$1/\tau = \alpha\eta\omega_0 a r_0^2 - \sqrt{\alpha^2\eta^2\omega_0^2\left(a r_0^2\right)^2 + 4\tilde{\mu}^2 - 4\tilde{\mu}\omega_0 a r_0^2}. \quad (15)$$

Using the value of the coupling parameter μ that can be extracted for very large interpillar distance L through the macrodipole approximation, we obtain a very rapid decrease of $1/\tau$ with interpillar distance L and eventually a phase locking time that tends to $\tau \longrightarrow \infty$ for large distances. It is important to note that interaction energy W_{int} becomes of the same order of magnitude as the room-temperature thermal energy kT at the interpillar distances L of about a single STNO diameter, thus the role of thermal effects in the phase locking of vortex STNOs has to be properly investigated.

In conclusion, we have demonstrated an efficient phase locking between two STNOs through a dipolar mechanism. We have succeeded in providing an accurate expression of the interaction energy between two vortice-based STNOs by comparing micromagnetic simulations to predictions of an analytical model based on coupled Thiele equations with dipole-dipole interacting forces. A major result is that the phase locking time τ is almost independent of the separation distances for values up to 1.6 μm before it increases very rapidly at larger distances. We emphasize also the critical importance of higher-order multipole terms for a correct description of the interaction energy, especially at shorter separation distances. Finally, our investigation will make it possible to design some optimized STNO ensembles for synchronization, which is a crucial step toward the development of a new generation of rf devices for telecommunication applications.

The work is supported by the EU Grant MASTER No. NMP-FP7 212257, RFBR Grants No. 10-02-01162 and No. 11-02-91067, CNRS PICS Russie No. 5743 2011, Federal Targeted Programs "Research and Development in Priority Areas of Russia's Scientific and Technological Complex 2007-2013", "Scientific and Scientific-Pedagogical Personnel of the Innovative Russia", and the ANR agency (VOICE PNANO-09-P231-36). F.A.A. acknowledges the Research Science Foundation of Belgium (FRS-FNRS) for financial support (FRIA grant).

[1] M. D. Stiles and J. Miltat, *Spin Dynamics in Confined Magnetic Structures III*, Topics in Applied Physics, Vol. 101 (Springer, New York, 2006), pp. 225–308.

[2] S. Kiselev, J. C. Sankey, I. N. Krivorotov, N. C. Emley, R. J. Schoelkopf, R. A. Buhrman, and D. C. Ralph, Nature (London) **425**, 380 (2003).

[3] A. Dussaux, B. Georges, J. Grollier, V. Cros, A. Khvalkovskiy, A. Fukushima, M. Konoto, H. Kubota, K. Yakushiji, S. Yuasa *et al.*, Nat. Commun. **1**, (2010).

[4] V. S. Pribiag, I. N. Krivorotov, G. D. Fuchs, P. M. Braganca, O. Ozatay, J. C. Sankey, D. C. Ralph, and R. A. Buhrman, Nat. Phys. **3**, 498 (2007).

[5] M. Manfrini, T. Devolder, J.-V. Kim, P. Crozat, N. Zerounian, C. Chappert, W. V. Roy, L. Lagae, G. Hrkac, and T. Schrefl, Appl. Phys. Lett. **95**, 192507 (2009).

[6] A. Ruotolo, V. Cros, B. Georges, A. Dussaux, J. Grollier, C. Deranlot, R. Guillemet, K. Bouzehouane, S. Fusil, and A. Fert, Nat. Nanotech. **4**, 528 (2009).

[7] A. Dussaux, A. Khvalkovskiy, J. Grollier, V. Cros, A. Fukushima, M. Konoto, H. Kubota, K. Yakushiji, S. Yuasa, K. Ando *et al.*, Appl. Phys. Lett. **98**, 132506 (2011).

[8] K. Y. Guslienko, J. Nanosci. Nanotech. **8**(6), 2745 (2008), http://www.ingentaconnect.com/content/asp/jnn/2008/00000008/00000006/art00003.

[9] A. V. Khvalkovskiy, J. Grollier, A. Dussaux, K. A. Zvezdin, and V. Cros, Phys. Rev. B **80**, 140401 (2009).

[10] A. Khvalkovskiy, A. Slavin, J. Grollier, K. A. Zvezdin, and K. Y. Guslienko, Appl. Phys. Lett. **96**, 022504 (2010).

[11] N. Locatelli, V. V. Naletov, J. Grollier, G. de Loubens, V. Cros, C. Deranlot, C. Ulysse, G. Faini, O. Klein, and A. Fert, Appl. Phys. Lett. **98**, 062501 (2011).

[12] J. Shibata, K. Shigeto, and Y. Otani, Phys. Rev. B **67**, 224404 (2003).

[13] A. Vogel, A. Drews, T. Kamionka, M. Bolte, and G. Meier, Phys. Rev. Lett. **105**, 037201 (2010).

[14] A. A. Awad, G. R. Aranda, D. Dieleman, K. Y. Guslienko, G. N. Kakazei, B. A. Ivanov, and F. G. Aliev, Appl. Phys. Lett. **97**, 132501 (2010).

[15] S. Barman, T. Kimura, Y. Fukuma, and Y. Otani, J. Phys. D **43**, 422001 (2010).

[16] H. Jung, Y.-S. Yu, K.-S. Lee, M.-Y. Im, P. Fischer, L. Bocklage, A. Vogel, M. Bolte, G. Meier, and S.-K. Kim, Appl. Phys. Lett. **97**, 222502 (2010).

[17] S. Sugimoto, Y. Fukuma, S. Kasai, T. Kimura, A. Barman, and Y. C. Otani, Phys. Rev. Lett. **106**, 197203 (2011).

[18] O. Sukhostavets, J. Gonzalez, and K. Guslienko, Appl. Phys. Express **4**, 065003 (2011).

[19] Y. Zhou, V. Tiberkevich, G. Consolo, E. Iacocca, B. Azzerboni, A. Slavin, and J. Akerman, Phys. Rev. B **82**, 012408 (2010).

[20] A. A. Thiele, Phys. Rev. Lett. **30**, 230 (1973).

[21] K. Metlov and K. Guslienko, J. Magn. Magn. Mater. **242-245**, 1015 (2002).

[22] K. Y. Guslienko and V. Novosad, J. Appl. Phys. **96**, 4451 (2004).

[23] W. Scholz, K. Y. Guslienko, V. Novosad, D. Suessa, T. Schrefla, R. W. Chantrell, and J. Fidlera, J. Magn. Magn. Mater. **266**, 155 (2003).

[24] K. Y. Guslienko, K. S. Buchanan, S. D. Bader, and V. Novosad, Appl. Phys. Lett. **86**, 223112 (2005).

[25] K. Y. Guslienko, X. F. Han, D. J. Keavney, R. Divan, and S. D. Bader, Phys. Rev. Lett. **96**, 067205 (2006).

[26] B. A. Ivanov and C. E. Zaspel, Phys. Rev. Lett. **99**, 247208 (2007).